Rock Mechanics and Rock Engineering (2022) 55:5845–5861
https://doi.org/10.1007/s00603-022-02941-5

ORIGINAL PAPER

A Time-Dependent Hydro-mechanical Coupling Model of Reservoir Sandstone During CO_2 Geological Storage

Hong Zheng[1] · Shiqi Cao[1,2] · Wei Yuan[3] · Quan Jiang[1] · Shaojun Li[1] · Guangliang Feng[1]

Received: 28 September 2021 / Accepted: 9 May 2022 / Published online: 29 June 2022

Abstract

Time-dependent deformation of rock affects the structural and hydrologic properties in terms of porosity and permeability, which can directly influence security and injectivity of CO_2 geological storages in a saline aquifer. To investigate the time-dependent response of deep saline aquifer subjected to CO_2 geological storage in terms of the permeability and deformation evolution of stratum rock skeleton under external stresses and pore fluid pressure, the rock permeability evolution under the flow-through of sodium chloride solution with mixed CO_2 and creep curves of reservoir rock sample was studied after long-term hydro-mechanical laboratory testing. Furthermore, the time-dependent hydro-mechanical coupling mathematical model, including the porous creep constitutive equation and the time-dependent relationship between volumetric deformation and porosity, was proposed to characterize the long-term influences of evolving permeability and deformation in a saline reservoir. To verify this time-dependent hydro-mechanical coupling model, the coupled multicomponent multiphase flow and geomechanical simulator TOUGH-FLAC could be applied with the embedded user-defined constitutive model of porous creep constitutive equation and the corrected permeability as function of volumetric strain in the external module. In general, calculated results are akin to observed results, and the time-dependent hydro-mechanical coupling model has practical value.

Highlights

- Reservoir porosity and permeability change with mechanical deformation as the results of alteration of pore pressureor lithostatic stress.
- As the results of long-term hydro-mechanical laboratory test show, both the deformation of reservoir rockand hydraulic conductivity are time-dependent.
- Long-term deformation characteristic of rock skeleton in saline reservoir couldbe evaluated via porous creep constitutive model.
- The capability of of iterative calculation process between Tough2 and Flac3Dis demonstrated on time-dependent hydro-mechanical coupled problems related to long-term geological storage of carbondioxide.

Keywords CO_2 geological storage · Hydro-mechanical coupling model · Time-dependent deformation · Strain-dependent permeability · TOUGH-FLAC

1 Introduction

As one of the main geological media for CO_2 sequestration at present, deep saline reservoirs are relatively widely accepted sites because of their larger storage capacities. Geological carbon storage units in deep saline aquifer are subjected to geostress and excess pore pressure induced by CO_2 injection (Ilgen et al. 2019). Consequently, a series of geomechanical risks such as the triggering of seismicity (Zoback and Gorelick 2012) and CO_2 leakage arising from activation of

✉ Hong Zheng
zhengh@whrsm.ac.cn

[1] State Key Laboratory for Geomechanics and Geotechnical Engineering, Institute of Rock and Soil Mechanics, Chinese Academy of Sciences, Wuhan 430071, China

[2] University of Chinese Academy of Sciences, Beijing 100049, China

[3] School of Civil Engineering, Shijiazhuang Tiedao University, Shijiazhuang 050043, China

faults and the destruction of caprock integrity (Vilarrasa and Carrera 2015) occur. Furthermore, besides caprock, geomechanical issues also arise in reservoir injectivity (Foroutan and Ghazanfari 2020). Aquifers consist of a rock stratum and underground fluid. An aquifer stratum, as porous medium, is sensitive to the fluid pressure (Coussy 2004). CO_2 injected into the target reservoir, as high-density, high-pressure fluid, will always cause geomechanical changes within and around a reservoir (Rutqvist 2012) that will result in rock deformation and porosity changes (Foroutan and Ghazanfari 2020). These restrict CO_2 storage space range in terms of pore distribution and groundwater seepage field of reservoir. Besides salt precipitation and mineral dissolution, variations of interparticle stress in the formation rock also alter the pore space size and pore connectivity and change the permeability to a significant extent, especially when the external load varies significantly. Therefore, hydromechanics, when coupled with geomechanics, plays a critical role in the security and injectivity of CO_2 geological storages.

Large amounts of long-term carbon dioxide geological storage represent an innovative scientific endeavor with considerable technical challenges (Seunghee et al. 2019). Since CO_2 sequestration is aimed at keeping the injected CO_2 in a permanent storage space in a deep saline aquifer, the evolution of rock deformation and permeability is valued for the efficiency and safety of CO_2 sequestration. Time-dependent deformation of rock exerts a potential influence on the structural and hydrologic properties in terms of porosity and permeability. Since the structural and hydrologic changes can directly affect the injection rate and pressure at CO_2 injection wells or CO_2 dissipation from the target storage reservoir due to leakage, this creep deformation has critical importance. For variational formation pore fluid pressure of CO_2 sequestration environment during such long periods, time-dependent compaction or expansion of the reservoir rock matrix is considered as rock matrix creep derived from the failure of intergranular cement and grains due to subcritical crack growth (Sharifzadeh et al. 2013).

Reservoir porosity and permeability change with mechanical deformation as the results of alteration of pore pressure or geostress. At the beginning of the CO_2 injection process, when CO_2 is squeezed into the primary pores of the reservoir rock, pore pressure and formation stress in the aquifer increase sharply, leading to the rock matrix shrinking. Meanwhile, the porosity and hydraulic conductivity of the formation increase with the enlarged pore volume. Following multiple CO_2 capture processes, the pore pressure dissipates due to the CO_2 dissolution and migration over a long period. As a result, the porosity and permeability decrease gradually. Furthermore, time-dependent deformation coupled with permeability evolution of the aquifer stratum can influence the range of CO_2 migration. As for the long-term injectivity and storage of saline reservoir, the pore capacity and connection of the stratum rock are sensitive to time-dependent deformation of the reservoir skeleton: with regard to security, the enlarged range of CO_2 migration over time is closely correlated with the permeability of the reservoir rock. Therefore, a thorough understanding of the hydro-mechanical coupling processes is demanded to quantify that time-dependent influence.

In view of the above, understanding the long-term response of porous rock in the reservoir to the external stresses and pore fluid is vital to engineering design in terms of hydraulic conductivity and creep deformation, especially for quantitative assessment of the long-term CO_2 storage behavior in terms of efficiency and security (Audigane et al. 2013). This requires a detailed study of multiple coupled phenomena displayed in the reservoir formation during geological sequestration, through experiments or numerical simulations of CO_2 injection into typical reservoir formations. Many researchers (Watanabe et al. 2010; Wang et al. 2009; Randolph and Saar 2011; Rutqvist et al. 2011; Morris et al. 2011; Lei et al. 2015) have studied reservoir mechanics combined with multicomponent multiphase flow to elucidate the role of porous media behavior for deep geological storage rock with carbon dioxide. Geomechanical-coupled modeling studies have proved that reservoir pressure induced by CO_2 injection changes may cause ground surface uplift or/and subsidence (Rutqvist et al. 2010) and correlated mechanical properties to porosity and permeability (Olden et al. 2012). Many laboratory investigations into the multiphase flow properties of CO_2 and underground fluid in reservoir rocks explored the petrophysical properties of typical reservoir rocks during multiphase flow of gas or/and liquid (Krevor et al. 2012); however, not many creep tests, conducted on porous rock as reservoir matrix, combined with multiphase flow, could describe the interaction of time-dependent mechanical deformation and brine mixed CO_2 migration. Most long-term experiments were implemented on the chemical mechanism based on the analyses of multiphase flow and reservoir rock, such as chemical creep phenomena (Hangx et al. 2013). While these responses in CO_2 geological storage exhibit long-term process activated by the hydraulic conductivity of the pore fluid (CO_2 and brine) and mechanics of reservoir rock, the present work covered a time-dependent hydro-mechanical coupling model on the basis of long-term hydro-mechanical laboratory test to investigate the long-term influence of evolving permeability and deformation on CO_2 geological storage in a deep saline aquifer.

Furthermore, numerical analysis plays a critical role in terms of describing the long-term hydro-mechanical coupling process on CO_2 geological storage in deep saline aquifer by time-dependent hydro-mechanical coupling models. Various geomechanical numerical modeling studies have been dedicated to the simulation of reservoir geomechanics

(Rutqvist et al. 2019). Rock skeleton deformation in the reservoir is a factor influencing reservoir injectivity, and storage in terms of permeability and porosity is particularly important (Foroutan et al. 2020). The success of carbon storage in deep saline reservoir depends on the ability of the reservoir to store carbon dioxide over at least thousands of years. That means, in view of reservoir properties, its hydraulic conductivity and pore water pressure determine the CO_2 migration. The pore fluid pressure, porosity, and permeability changed in space and time, from injection to post-stabilization and from near the well-bore to far-field conditions. Different areas of sequestration sites will experience different hydro-mechanical coupling problems in different phases, such as reactivating fracture networks that develop to form leakage pathways in the caprock and compromise the wellbores' cement by mechanical or chemical effects. In this paper, the long-term hydro-mechanical coupling process was simulated by elucidating the relationship between time-dependent deformation of the reservoir rock and the evolution of porosity and permeability with the application of TOUGH-FLAC simulator.

In carbon storage in deep saline reservoir, the target quantity of carbon dioxide is most readily achieved through the injection at the supercritical state. High injection pressure and high-density carbon dioxide trigger the rapid increase of excess pore pressure near the injection well: this gives rise to voluminous CO_2 dissolution and migration from the injection unit to the far-field region, as well as its long time scale depending on the pore pressure with a gradually reduced trend to a stable state. To reveal the evolution mechanism within the reservoir rock porosity and permeability during CO_2 dissolution and migration, both the laboratory experiments and numerical simulation described herein were designed to investigate the effects of multiphase flow (i.e. NaCl solution with mixed CO_2) on the time-dependent mechanical and hydraulic properties of the reservoir rock.

2 Experimental Investigation

In the process of carbon dioxide geological storage, when vast amounts of carbon dioxide can be injected into the aquifer of the underground geological storage site, the physico-chemical properties of the water–rock system will be affected, and its evolution mechanism directly influences the storage space, transport capacity, and mechanical stability of the reservoir formation. For the purpose of experimental mechanism research, the following laboratory test is dedicated to revealing the evolution of transport and mechanical properties of reservoir rock samples.

To analyze the time-dependent hydro-mechanical coupling process of CO_2 capture in brine reservoirs, rock creep testing combined with permeability determination was implemented with porous sandstone and salt water.

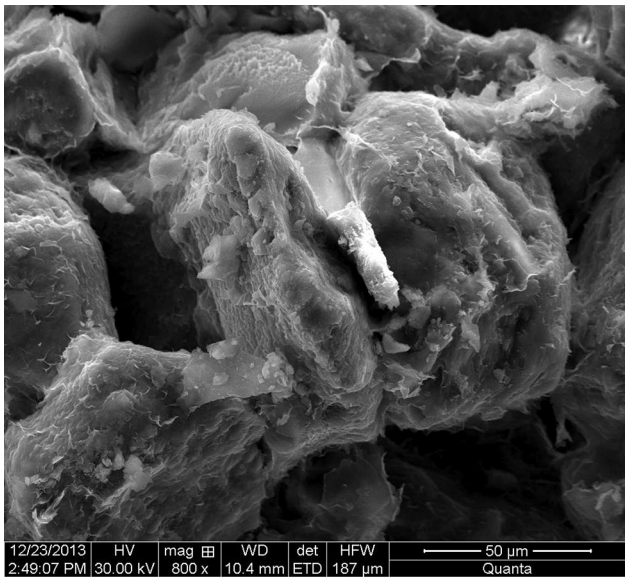

Fig. 1 SEM image (800 × magnification): porous sandstone

2.1 Experimental Materials

To provide insight into the influences of salt water flow mixed CO_2 on reservoir rock and its time-dependent deformation and permeability, sandstone with porosity of 22.15% was selected as a reservoir similar material. Pore radius, pore density, and pore-throat ratio influence reservoir permeability to different extents. Therefore, it is necessary to observe the pore network of porous sandstone when using an SEM to investigate an internal cross section of porous sandstone. From the investigation results, the micrograph of the sandstone specimen at 800 times magnification is shown in Fig. 1.

As can be seen from Fig. 1, porous sandstone consists of mineral particles with uneven particle size and intergranular cement. Sandstone particles have high roundness and fine internal pore connectivity. As the mechanical combined response of pore fluid pressure and formation stress, the rock matrix is deformed in a complex manner and its stiffness depends on the pore network structure mechanical properties of the porous skeleton.

Referring to the main components of the underground salt water in deep saline aquifers, sodium chloride is prevalent and accounts for most of the salinity. The sample water was represented by a 0.1-mol/L sodium chloride solution as a substitute for pore salt water of reservoir in laboratory test.

The laboratory test scheme should consider the formation stress in the reservoir, underground fluid pressure, and CO_2 content, which provide evidence for the selection of

triaxial loading on rock sample, and seepage pressure gradient and multiphase fluid composition of pore fluid in the experiment, respectively. In the process of CO_2 storage in the deep reservoir, the pore pressure and CO_2 content in pores constantly vary with space and time due to CO_2 dissolution and diffusion. From the perspective of time scale, the excess pore water pressure tends to be stable in the long term. From the perspective of spatial scale, the pore pressure gradually decreases from the injection area to the far-field area. In addition, the CO_2 content in pore fluid is affected by its solubility in salt water, which depends on the temperature and pressure. To avoid the interference of multiple influencing factors, the CO_2 content of the initial mixed fluid and the injection pressure are kept constant in the laboratory test.

2.2 Long-Term Hydro-mechanical Laboratory Testing

Long-term hydro-mechanical laboratory tests were conducted on the multi-field coupling test system with the triaxial cell as the core component; its outlet was connected to the servo-motor controlled pump for collecting and obtaining the outflow data, while the inlet was connected to the reactor container with an NaCl solution containing CO_2.

Fig. 2 Cylindrical specimen in triaxial loading system for creep tests

Triaxial creep tests with the flow-through of NaCl solution mixed CO_2 were implemented at a constant temperature of 25 °C. Before each test, to obtain sandstone with in-pore salt water, dry sandstone specimens were saturated with 0.1 mol/L NaCl solution using the vacuum suction method suggested by the ISRM. This is to ensure better simulation of the salt groundwater environment. Following this, the cylinder saturated specimen was put in a triaxial loading system with the radial pressure of 10 MPa and the axial stress of 20 MPa, successively (Fig. 2). With the initiation of the reaction, pure CO_2 was constantly mixed with the NaCl solution at 25 °C at a pressure of 1 MPa until the solution was saturated with CO_2. The reactor was maintained at that constant temperature and pressure in the reactor, as well as the concentration of influent NaCl solution. Under constant conditions, the dissolved CO_2 and water achieved chemical equilibrium in this process of dissolution and ionization. Then, the CO_2 saturated NaCl solution, mixed well, was injected by means of the reactor container at a permeation pressure of 1 MPa and a constant pressure difference was maintained, which means the difference in pore pressure between the inlet and outlet of specimen in the triaxial loading system was 1 MPa. The aqueous solubility of CO_2 was decreased with increasing temperature and salinity and increased with increasing pressure. Therefore, from inlet to outlet, excess CO_2 gradually escaped out of the solution.

The equipment automatically collected displacement data according to the acquisition frequency, while the water flow at set intervals from the outlet was recorded during the following 120 h. To measure and obtain the displacement along the radial and axial directions of the rock specimen, circular deformation-measuring devices and a linear variable differential transducer in the axial direction were used in the triaxial loading system for creep tests. The circular deformation-measuring device was mainly composed of spring steel and resistance strain gauges. Calibration showed that the linear ranges and linearities of circular deformation-measuring device and LVDT are acceptable: the axial and lateral deformations are accurate to 10^{-4} mm and 10^{-6} mm, respectively. According to the axial strain ε_1 and lateral strain ε_3, the volumetric strain e_{vol} was obtained by summing twice the lateral strain and the axial strain, i.e. $e_{vol} = \varepsilon_1 + 2\varepsilon_3$.

As the measurement results of triaxial creep tests with the flow-through of NaCl solution mixed with CO_2, the axial, lateral, and volumetric creep time curves of specimen are shown in Fig. 3a. With the application of a servo-motor controlled pump as an effluent collection device, the liquid flux at the outlet under steady seepage through the sample was measured and its hydraulic conductivity was calculated using Darcy's law. The hydraulic conductivity during the flow-through experiment is shown in Fig. 3b.

In Fig. 3, under a confining pressure of 10 MPa, an axial stress of 20 MPa, and a seepage pressure of 1 MPa, the axial,

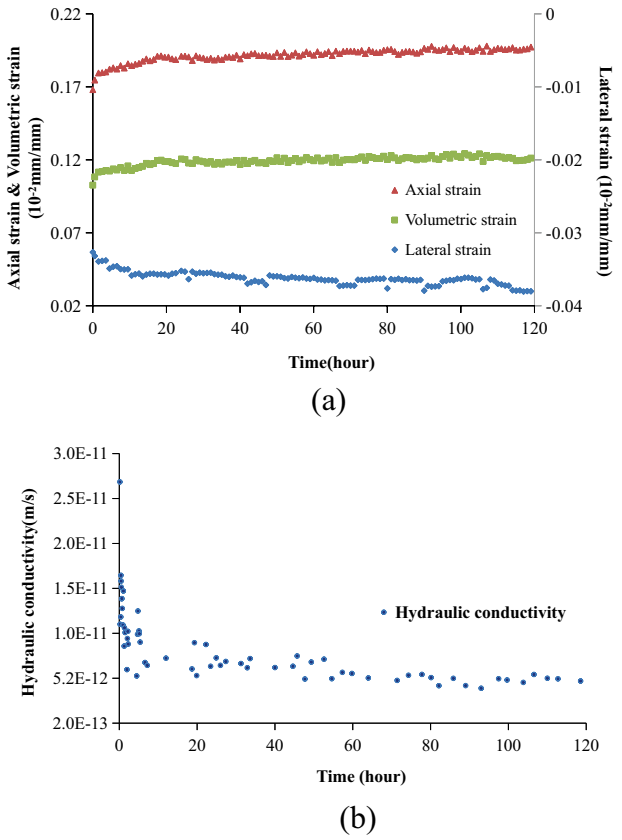

Fig. 3 **a** The axial, lateral, and volumetric creep time curves and **b** hydraulic conductivity–time curves of sandstone specimen with the flow-through of NaCl solution mixed with CO_2 (confining pressure: 10 MPa; axial stress: 20 MPa; seepage pressure: 1 MPa)

lateral, and volumetric deformation increased with time. In addition, the hydraulic conductivity of the sandstone specimen under the seepage of NaCl solution mixed with CO_2 diminished with time under a constant stress. This decreasing evolution of hydraulic conductivity was time dependent and gradually decelerated.

2.3 Analysis of the Results

In previous studies, rock samples displayed similar long-term deformation behavior characterized by time-dependent deformation due to various experimental parameters, such as effective stress, mineralogy, internal structure, and fluid flow rate. These experiments involved a constant pore pressure and external load to reveal the time-dependent hydro-mechanical coupling process occurring during the flow-through of the NaCl solution mixed CO_2.

The porosity and hydraulic conductivity in a reservoir are closely related to the deformation of reservoir rock. In view of the porous material, a reservoir is composed of a formation skeleton and pore fluid. The compressible rock skeleton demonstrates time-dependent creep deformation (Fig. 3). Differing from the excess pore water pressure and quick seepage in the reservoir in the CO_2 injection phase (Guen 2007; Rutqvist et al. 2016), after the injection pressure dissipation process is implemented, the steady flow of mixed CO_2 and groundwater spread to far-field flow. As the key concern of CO_2 storage safety in the long term, CO_2 migration and the range thereof depend on the rate of gas transport and time. Referring to long-term hydro-mechanical laboratory test, both the deformation of reservoir rock and hydraulic conductivity are time dependent. This means that the evolution of creep of the rock skeleton and permeability is relevant: more theoretical work was expounded subsequently to reveal the relationship between the rock skeleton creep deformation and its hydraulic conductivity.

Confined to the application scope of analytic solution by Darcy's law, the hydraulic conductivity of the liquid phase in outflow, without a gas phase, was calculated, and the hydraulic conductivity of the liquid phase demonstrated the ability of the liquid phase to pass through the pore skeleton. Due to the mutual interference and capillary resistance of each phase during the flow process, the sum of the hydraulic conductivities of each phase was less than the absolute hydraulic conductivity. By considering the complex phase transition, the multicomponent multiphase flow simulation method could provide numerical results of hydraulic conductivity for both gas and liquid phases. Further numerical work was conducted to describe the evolution of hydraulic conductivity.

3 Development and Implementation of a Time-Dependent Hydro-mechanical Coupling Model

Based on the long-term hydro-mechanical laboratory test on a sandstone specimen with the flow-through of sodium chloride solution with mixed CO_2, the evolution of the mechanical and hydraulic characteristics of the rock skeleton was clarified. A theoretical model was applied to reveal the co-evolution in this hydro-mechanical process. To quantify these couplingproperties at a scale, flow and skeleton deformation were described by continuum-scale physics. However, their time variabilityrepresents an additional challenge in the theoretical model.

Mechanical deformation characteristics of reservoir rock are directly dependent on its skeleton. This section is aimed at a discussion of the time-dependent mechanical behavior of the porous rock skeleton in a reservoir. Creep of the rock skeleton is governed by compressible skeletal structures, their mineral composition and degree of cementation, which can be represented in this creep model by choice of mechanical parameters; therefore, a sufficient mechanical constitutive model should be proposed to reflect rock-skeleton creep

during the hydro-mechanical coupling processes. For porous rock, time-dependent compaction or expansion of rock skeleton depends on the combined action of stress and pore pressure. In general, the deformation increment of rock-skeleton creep is derived from pore deformation, grain failure, and grains separated from cement by crack initiation and propagation, as well as intergranular pressure solution and dissolution–precipitation processes at the free face of each pore. In the present research, as the dominant mechanical mechanisms contribute to hydro-mechanical coupling process in porous reservoir, the chemical effect on the long-term deformation is ignored.

3.1 Porous Creep Model

In view of the porous material, saline reservoirs used as CO_2 storage sites consist of rock skeleton and underground salt water with CO_2 in its pores: the rock skeleton includes pores and a solid matrix. The mechanical deformation characteristics of reservoir rock are directly dependent on its skeleton. Since volumetric deformation and shear deformation as two deformation mechanisms in traditional solid mechanics also could be applied to the porous rock skeleton, giving its volumetric deformation as attributed to the expansion and contraction of the pore structure under the hydrostatic stress component, it leads to pore collapse, cement debonding, and coalescence of adjacent pores, while its shear deformation is due to the distorted pore shape and solid matrix distortion under the deviatoric stress component. As the outcomes of two deformation mechanisms, the shape, size, and connectivity of the pore structure are altered. Many researchers have investigated the creep constitutive model applicable to various geologic materials. Compared with other creep constitutive models of geologic materials—such as empiricism and a thermodynamic framework—the elemental creep model is better suited to numerical calculation in such cases owing to its easy access to model parameters.

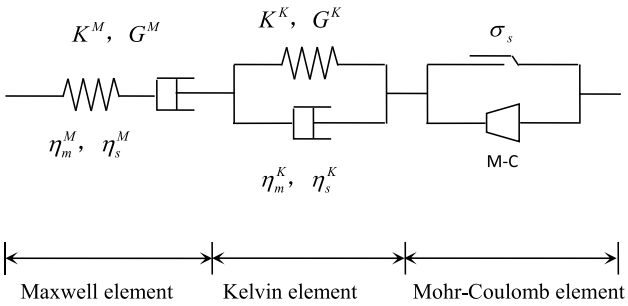

Fig. 4 Schematic representation of the porous creep model

To describe the time-dependent deformation of porous rock in reservoir, including the volumetric part and shear part, the porous creep model is composed of a Maxwell element, a Kelvin element, and a Mohr–Coulomb element (Fig. 4). The parameters in the creep model are listed in Table 1.

After entering the plastic stage, the Mohr–Coulomb plastic element in the model begins to play a role, and its Mohr–Coulomb yield envelope contains two criteria based on shear and tensile stresses. The yield criterion is $f = 0$, combined with the principle of effective stress, such that:

$$f = \sigma_1' - \sigma_3' N_\varphi + 2c\sqrt{N_\varphi}. \tag{1}$$

Tensile yield is represented as:

$$f = \sigma^t - \sigma_3', \tag{2}$$

where c is the apparent cohesion; $N_\varphi = (1 + \sin\varphi)/(1 - \sin\varphi)$, and φ is the friction angle; σ^t denotes the tensile strength; σ_1' and σ_3' are the maximum and minimum principal effective stresses, respectively.

The maximum and minimum principal effective stresses are expressed as $\sigma_1' = \sigma_1 - b_1 p$ and $\sigma_3' = \sigma_3 - b_3 p$, where σ_1 and σ_3 are the maximum and minimum principal stresses, p is the pore fluid pressure, and b_1 and b_3 are the corresponding effective stress coefficients. In the isotropic case, $b_1 = b_3$.

The Mohr–Coulomb criterion is used with a non-associated flow rule, and its potential function g is defined in the following form:

$$g = \sigma_1' - \sigma_3' N_\psi \quad \text{(shear failure)}, \tag{3}$$

Table 1 Parameters in the creep model

Symbol	Meaning
K^{M}	Bulk moduli of the elastic part in a Maxwell element
G^{M}	Shear moduli of the elastic part in a Maxwell element
$\eta_{\mathrm{m}}^{\mathrm{M}}$	Volumetric viscosity coefficients of the viscous part in a Maxwell element
$\eta_{\mathrm{s}}^{\mathrm{M}}$	Deviatoric viscosity coefficients of the viscous part in a Maxwell element
K^{K}	Bulk moduli of the elastic part in a Kelvin element
G^{K}	Shear moduli of the elastic part in a Kelvin element
$\eta_{\mathrm{m}}^{\mathrm{K}}$	Volumetric viscosity coefficients of the viscous part in a Kelvin element
$\eta_{\mathrm{s}}^{\mathrm{K}}$	Deviatoric viscosity coefficients of the viscous part in a Kelvin element

Table 2 The volumetric and deviatoric strain rates of different elements in the porous creep model of sandstone under spherical and deviatoric stress

	Volumetric strain rate $\dot{e}_{\mathrm{vol}}$	Deviatoric strain rate $\dot{e}_{ij}$
Maxwell element	$\dot{e}_{\mathrm{vol}}^{\mathrm{M}} = \frac{\dot{\sigma}'_{\mathrm{m}}}{K^{\mathrm{M}}} + \frac{\sigma'_{\mathrm{m}}}{\eta_{\mathrm{m}}^{\mathrm{M}}}$	$\dot{e}_{ij}^{\mathrm{M}} = \frac{\dot{S}'_{ij}}{2G^{\mathrm{M}}(1-\omega_{\mathrm{s}})} + \frac{S'_{ij}}{2\eta_{\mathrm{s}}^{\mathrm{M}}(1-\omega_{\mathrm{s}})}$
Kelvin element	$\sigma'_{\mathrm{m}} = \eta_{\mathrm{m}}^{\mathrm{K}}\dot{e}_{\mathrm{vol}}^{\mathrm{K}} + K^{\mathrm{K}}e_{\mathrm{vol}}^{\mathrm{K}}$	$S'_{ij} = 2\eta_{\mathrm{s}}^{\mathrm{K}}\dot{e}_{ij}^{\mathrm{K}} + 2G^{\mathrm{K}}e_{ij}^{\mathrm{K}}$
Mohr–Coulomb plastic element	$\dot{e}_{\mathrm{vol}}^{\mathrm{p}} = \lambda\left[\frac{\partial g}{\partial \sigma'_{11}} + \frac{\partial g}{\partial \sigma'_{22}} + \frac{\partial g}{\partial \sigma'_{33}}\right]$	$\dot{e}_{ij}^{\mathrm{p}} = \lambda\frac{\partial g}{\partial \sigma'_{ij}} - \frac{1}{3}\dot{e}_{\mathrm{vol}}^{\mathrm{p}}\delta_{ij}$
Total strain rate	$\dot{e}_{\mathrm{vol}} = \dot{e}_{\mathrm{vol}}^{\mathrm{K}} + \dot{e}_{\mathrm{vol}}^{\mathrm{M}} + \dot{e}_{\mathrm{vol}}^{\mathrm{p}}$	$\dot{e}_{ij} = \dot{e}_{ij}^{\mathrm{K}} + \dot{e}_{ij}^{\mathrm{M}} + \dot{e}_{ij}^{\mathrm{p}}$

$$g = -\sigma'_3 \quad \text{(tensile failure)}, \tag{4}$$

where $N_\psi = (1+\sin\psi)/(1-\sin\psi)$, ψ is the angle of dilation.

According to the deformation characteristics of porous sandstone under different stress elements, the total strain rate is the sum of the volume strain rate and deviatoric strain rate, which can constitute the deformation of three elements in this model under spherical stress and deviatoric stress, respectively. Therefore, the strain rate is expressed as:

$$\dot{\varepsilon}_{ij} = \frac{\dot{e}_{\mathrm{vol}}}{3}\delta_{ij} + \dot{e}_{ij}. \tag{5}$$

The volumetric strain rates and deviatoric strain rates of the Maxwell element, Kelvin element, and Mohr–Coulomb plastic element under spherical and deviatoric stress are summarized in Table 2.

In Table 1, λ is the parameter that is not 0 only at the stage of plastic flow and $f = 0$ is determined by the plastic yield condition.

Different from the conventional creep model, this porous creep model considers the volumetric time-dependent strain under spherical stress state. As a result, the three-dimensional constitutive relationship of the viscoelastic part under spherical stress state is obtained as:

$$\sigma'_{\mathrm{m}} + \left(\frac{\eta_{\mathrm{m}}^{\mathrm{M}}}{K^{\mathrm{M}}} + \frac{\eta_{\mathrm{m}}^{\mathrm{M}} + \eta_{\mathrm{m}}^{\mathrm{K}}}{K^{\mathrm{K}}}\right)\dot{\sigma}'_{\mathrm{m}} + \frac{\eta_{\mathrm{m}}^{\mathrm{M}}\eta_{\mathrm{m}}^{\mathrm{K}}}{K^{\mathrm{M}}K^{\mathrm{K}}}\ddot{\sigma}'_{\mathrm{m}} = \eta_{\mathrm{m}}^{\mathrm{M}}\dot{e}_{\mathrm{vol}} + \frac{\eta_{\mathrm{m}}^{\mathrm{M}}\eta_{\mathrm{m}}^{\mathrm{K}}}{K^{\mathrm{K}}}\ddot{e}_{\mathrm{vol}}, \tag{6}$$

where $\dot{\sigma}'_{\mathrm{m}}$ and $\ddot{\sigma}'_{\mathrm{m}}$ are the first and second differential of the mean effective stress with respect to time; $\dot{e}_{\mathrm{vol}}$ and $\ddot{e}_{\mathrm{vol}}$ are the first and second differential volumetric strains with respect to time, respectively.

Similarly, the three-dimensional constitutive relationship of the viscoelastic part under deviatoric stress state is expressed as:

$$S'_{ij} + \left(\frac{\eta_{\mathrm{s}}^{\mathrm{M}}}{G^{\mathrm{M}}} + \frac{\eta_{\mathrm{s}}^{\mathrm{M}} + \eta_{\mathrm{s}}^{\mathrm{K}}}{G^{\mathrm{K}}}\right)\dot{S}'_{ij} + \frac{\eta_{\mathrm{s}}^{\mathrm{M}}\eta_{\mathrm{s}}^{\mathrm{K}}}{G^{\mathrm{M}}G^{\mathrm{K}}}\ddot{S}'_{ij} = 2\eta_{\mathrm{s}}^{\mathrm{M}}\dot{e}_{ij} + \frac{2\eta_{\mathrm{s}}^{\mathrm{M}}\eta_{\mathrm{s}}^{\mathrm{K}}}{G^{\mathrm{K}}}\ddot{e}_{ij}, \tag{7}$$

where $\dot{S}'_{ij}$ and $\ddot{S}'_{ij}$ are the first and second differential deviatoric effective stresses with respect to time; $\dot{e}_{ij}$ and $\ddot{e}_{ij}$ denote the first and second differential shear strains with respect to time, respectively.

Furthermore, before entering the plastic yield stage, the sandstone is in a viscoelastic state; the creep constitutive equation of this porous creep model is given by:

$$\begin{aligned}\varepsilon_{ij}(t) = &\left(\frac{\sigma'_{\mathrm{m}}}{3K^{\mathrm{M}}} + \frac{\sigma'_{\mathrm{m}}}{3\eta_{\mathrm{m}}^{\mathrm{M}}}t + \frac{\sigma'_{\mathrm{m}}}{3K^{\mathrm{K}}}\left(1 - e^{-\frac{K^{\mathrm{K}}}{\eta_{\mathrm{m}}^{\mathrm{K}}}t}\right)\right)\delta_{ij} \\ &+ \frac{S'_{ij}}{2G^{\mathrm{M}}} + \frac{S'_{ij}}{2\eta_{\mathrm{s}}^{\mathrm{M}}}t + \frac{S'_{ij}}{2G^{\mathrm{K}}}\left(1 - e^{-\frac{G^{\mathrm{K}}}{\eta_{\mathrm{s}}^{\mathrm{K}}}t}\right).\end{aligned} \tag{8}$$

Once it enters the plastic stage, plastic strain needs to be added according to the Mohr–Coulomb flow rule.

3.2 Determination and Calibration of the Model Parameters

The porous creep model includes eight parameters as given in Eq. (8): four parameters were considered to describe the volumetric behavior, such as the bulk moduli in Maxwell elements and Kelvin elements, and the volumetric viscosity coefficients in Maxwell elements and Kelvin elements, while four parameters were used for deviatoric behavior, such as the shear moduli of the elastic part in Maxwell elements and Kelvin elements, and the deviatoric viscosity coefficients of the viscous part in Maxwell elements and Kelvin elements. These two suites of parameters were, respectively, determined by volumetric creep data and deviatoric creep data.

The bulk moduli and shear moduli of the elastic part in the Maxwell element were obtained from Eq. (9), which are derived from Eq. (8) with the initial volumetric strain, and initial axial deviatoric strain. Other uncertain parameters were obtained by minimizing the objective function of n fitting points of volumetric creep data and deviatoric creep data at the beginning. Taking the uncertain volumetric parameters as the example, $\Psi_{\mathrm{n}}\left(K^{\mathrm{K}}, \eta_{\mathrm{m}}^{\mathrm{M}}, \eta_{\mathrm{m}}^{\mathrm{K}}\right)$ is the objective function used to find the optimal solution for the three parameters representing the volumetric behavior.

$$e_{\mathrm{vol}}(t=0) = \frac{\sigma'_{\mathrm{m}}}{K^{\mathrm{M}}}; \quad e_{ij}(t=0) = \frac{S'_{ij}}{2G^{\mathrm{M}}}, \tag{9}$$

$$\Psi_{\mathrm{n}}(K^{\mathrm{K}}, \eta_{\mathrm{m}}^{\mathrm{M}}, \eta_{\mathrm{m}}^{\mathrm{K}}) = \sqrt{\sum_{i=1}^{n} \left(\frac{\hat{e}_{\mathrm{vol}(i)} - e_{\mathrm{vol}(i)}}{e_{\mathrm{vol}(i)}} \right)^2 \Big/ n}, \tag{10}$$

where $\hat{e}_{\mathrm{vol}(i)}$ is the simulated result of i group data, $e_{\mathrm{vol}(i)}$ denotes the experimental data, and n represents the number of fitting points.

Taking the volumetric parameters in the experiment as the reference value, the influences of volumetric parameters with deviations of ± 15% and ± 30% are shown in Fig. 5a–c.

Figure 5a–c shows that three uncertain volumetric parameters are sensitive to volumetric creep in different stages. Rock creep is divided into stable creep and unsteady creep. For stable creep, deformation changes over time, but after the transition creep stage, the deformation rate tends to zero, and the deformation eventually tends to a stable value without causing failure. However, during unsteady creep, deformation develops continuously with time, and the typical deformation process is transitional creep, steady creep, and accelerated creep, which eventually lead to failure.

As shown in Fig. 5a, the volumetric viscosity coefficient in Kelvin elements is the sensitive parameter in the transition creep stage and affects the duration of the first stage. The smaller its value, the earlier does its creep enter the stable stage. As shown in Fig. 5b, the bulk moduli in Kelvin elements can be the sensitive parameter in the transition creep stage and stable creep stage and affect the critical deformation between the transition creep stage and the stable creep stage. The smaller the bulk moduli in Kelvin elements, the larger is the critical deformation. As shown in Fig. 5c, the volumetric viscosity coefficient in Maxwell elements is the sensitive parameter in the stable creep stage and affects the slope of the curve in the stable creep stage. The smaller its value, the larger is the slope of the curve in the stable creep stage. The deviatoric uncertain parameters play similar roles in the deviatoric part of Eq. (8) as the volumetric parameters do in the volumetric part; therefore, a similar influence on the creep curve should be considered for the deviatoric uncertain parameters. Since the plastic part is subject to the Mohr–Coulomb criterion, the determination of plastic parameters without innovation is omitted.

Besides the model parameters, the creep curve also depends on stress; so, the influences of parameters in different creep stages under different stress states vary and should be confirmed by analysis and further parametric calibration.

To improve the prediction accuracy of time-dependent deformation evolution, the sensitivity analysis is crucial for parameter calibration. For a system containing k factors, its system characteristic is defined as P^* under a certain benchmark condition $\alpha^* = \{\alpha_1^*, \alpha_2^*, \cdots, \alpha_k^*\}$. When each influencing factor changes within its possible range of values, the system characteristic P will deviate from the reference state P^*. The influence of this parameter on the system characteristics is determined by observing the change of system characteristic P caused by certain changes in the influencing factors; therefore, the sensitivity function is expressed as:

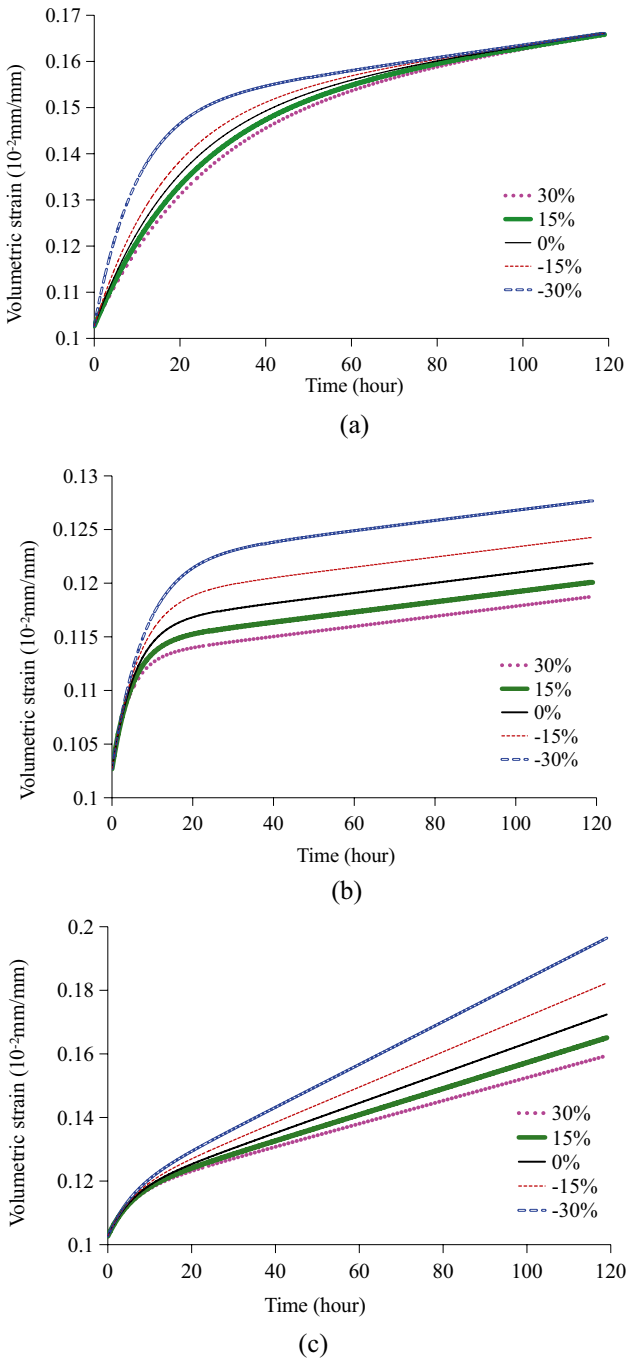

Fig. 5 The influence of **a** volumetric viscosity coefficient in Kelvin elements, **b** bulk moduli in Kelvin elements, and **c** volumetric viscosity coefficient in Maxwell elements with deviations of ± 15% and ± 30%

$$S_i(\alpha_i) \cong \left(\frac{|\Delta P|}{P^*}\right) \Big/ \left(\frac{|\Delta \alpha_i|}{\alpha_i^*}\right) = \left|\frac{\Delta P}{\Delta \alpha_i}\right| \cdot \frac{\alpha_i^*}{P^*} \quad i = 1, 2, \cdots, k, \tag{11}$$

where α_i^* is the factor α_i under benchmark conditions; $\Delta\alpha_i$ is the difference from the benchmark condition value of the factor α_i. P^* is the system characteristic; ΔP denotes the difference from the system benchmark characteristic. $S_i(\alpha_i)$ is the sensitivity of the factor α_i.

This porous creep model is calibrated based on sensitivity analysis results by adjusting only the most sensitive parameters, and the root mean square relative error is adopted as an objective function to calibrate each parameter.

$$\Phi_{\mathrm{m}}(\alpha_{\mathrm{most}}) = \sqrt{\sum_{i=1}^{m} \left(\frac{\hat{\chi}_i - \chi_i}{\chi_i}\right)^2 \Big/ m}, \tag{12}$$

where $\Phi_{\mathrm{m}}(\alpha_{\mathrm{most}})$ is the root mean square relative error, $\hat{\chi}_i$ denotes calculated data, χ_i refers to observed data, and m $(m > n)$ represents the total number of measurement points. If $\Phi_{\mathrm{m}}(\alpha_{\mathrm{most}})$ is minimized, the parameter calibration is considered complete.

3.3 Porosity and Permeability as Time-Dependent Variables

The deformable rock skeleton in the reservoir is a porous material and the porosity is sensitive to deformation and the permeability of the rock. The decrease in permeability with increased confining pressure has been well demonstrated for a great variety of reservoir rocks and many relationships linking porosity/permeability and deformation or stress have been developed. However, fluid pressure derives from the injection well and propagates to the reservoir during carbon storage in deep saline aquifers, changing the pore pressures therein. This pore pressure dissipation, as a long-term process, depends on the mechanical and physical properties of reservoir formation and the prevailing multiphase flow characteristic. The influence of long-term deformation on porosity and permeability is an issue of critical concern.

Since pore geometry is the fundamental control of stress-/strain-dependent permeability in porous reservoirs, for long-term evolution, both porosity and permeability are time-dependent variables related to stress/strain. It should be noted that, in spite of the precipitation and dissolution behaviors in the rock matrix also influencing the skeleton porosity and permeability, compared with the stress-dependent part, the chemically induced changes in permeability are ignored.

According to the definition of porosity φ, it is the ratio of pore space volume V_p to the total volume of the skeleton V_t as $\varphi = \frac{V_p}{V_t}$. In mechanics, volumetric deformation ε_v is described as the ratio of volume increment ΔV_t to initial volume V_t. For a porous material, the contribution to the volume increment in the skeleton comes from the pore and solid matrix. In view of poro-mechanics (Coussy 2004), the volume balance relationship is expressed as:

$$\varepsilon_{\mathrm{v}} = (1 - \varphi_0)\varepsilon_{\mathrm{v}}^{\mathrm{s}} + \varphi - \varphi_0, \tag{13}$$

where $\varepsilon_{\mathrm{v}}^{\mathrm{s}}$ is the volume dilation undergone by the solid matrix, and φ and φ_0 represent the porosity and initial porosity.

Under the assumption that the pores are absolutely connected, the volume change of solid grains is negligible, which means that the matrix can be considered as incompressible. Accordingly, we set $\varepsilon_{\mathrm{v}}^{\mathrm{s}} = 0$ in Eq. (13), giving:

$$\varepsilon_{\mathrm{v}} = \varphi - \varphi_0. \tag{14}$$

This means the change of the porosity during creep then corresponds to the skeleton volumetric deformation. For long-term deformation, creep volumetric strain reflects the change in porosity with time. Since permeability and porosity are exponentially related (Rutqvist et al. 2002), combined with Eq. (13), permeability as a function of volumetric strain can be derived as:

$$k = k_0 \cdot \exp\left(\frac{c\varepsilon_{\mathrm{v}}}{\varphi_0}\right), \tag{15}$$

where k_0 denotes the initial permeability and c is a constant coefficient.

4 Coupling Simulation by TOUGH-FLAC

TOUGH-FLAC links the multicomponent multiphase flow simulator TOUGH2 with the geomechanical simulator FLAC^{3D}. Tough2 is a relatively mature software, and its state module ECO$_2$N is widely used in the calculation and analysis of multiphase flow of CO_2 brine mixtures. In consequence, Tough2 combined with FLAC^{3D} provides the ability to model the geomechanics of CO_2 geological seals (Rutqvist 2011). The application of Tough2-FLAC^{3D} to study time-dependent hydro-mechanical coupling process of CO_2 sequestrate in saline aquifer requires some modifications to the simulator: the changes in volumetric deformation with time are considered in the creep model of porosity as a secondary development tool in Flac^{3D}. The external coupling modules should be corrected to reflect the relationship between rock skeleton deformation and reservoir hydraulic conductivity. Here, we conducted a coupling calculation of the reservoir creep process and time-dependent changes in permeability during the process of CO_2 injection with the application of the TOUGH-FLAC coupled program. Besides, the time-dependent hydro-mechanical

coupling model which considers rock skeleton volumetric creep and time evolution of permeability is expected to be adopted to describe the long-term hydraulic characteristics and mechanical stability during/after injection of CO_2 into a brine reservoir.

4.1 Numerical Simulation of Porous Creep Model in FLAC^{3D}

Before presenting the development and implementation of a time-dependent hydro-mechanical coupling model into the coupled multicomponent multiphase flow and geomechanical software TOUGH-FLAC, a constitutive equation of porous creep model was embedded in FLAC^{3D} to deduce the long-term deformation of a porous reservoir rock.

FLAC^{3D}, when edited by object-oriented C++, is convenient and simple with regard to the addition of a user-defined constitutive model. To demonstrate the creep properties of porous sandstone, the creep constitutive model was programmed to incorporate this secondary development of the Burger-creep visco-plastic model. On that basis, the *.h* and .cpp files were modified to generate the new dynamic link library file as then used for subsequent numerical calculations.

According to the finite difference method, differential forms of the creep constitutive equation for this porous creep model can be derived from relationships in Table 1. By using the superscripts N and O to refer to the new and old data in each time step, the new volumetric strain in the Kelvin element is expressed as:

$$e_{\mathrm{vol}}^{\mathrm{K,N}} = \frac{1}{A_{\mathrm{m}}}\left[B_{\mathrm{m}} e_{\mathrm{vol}}^{\mathrm{K,O}} + \frac{\Delta t}{2\eta_{\mathrm{m}}^{\mathrm{K}}}\left(\sigma'^{\mathrm{N}}_{\mathrm{m}} + \sigma'^{\mathrm{O}}_{\mathrm{m}}\right)\right], \tag{16}$$

where $A_{\mathrm{m}} = 1 + \frac{K^{\mathrm{K}}\Delta t}{2\eta_{\mathrm{m}}^{\mathrm{K}}}, B_{\mathrm{m}} = 1 - \frac{K^{\mathrm{K}}\Delta t}{2\eta_{\mathrm{m}}^{\mathrm{K}}}$.

Similarly, the new deviatoric strain in the Kelvin element is given as:

$$e_{ij}^{\mathrm{K,N}} = \frac{1}{A_{\mathrm{s}}}\left[B_{\mathrm{s}} e_{ij}^{\mathrm{K,O}} + \frac{\Delta t}{4\eta_{\mathrm{s}}^{\mathrm{K}}}\left(S'^{\mathrm{N}}_{ij} + S'^{\mathrm{O}}_{ij}\right)\right], \tag{17}$$

where $A_{\mathrm{s}} = 1 + \frac{G^{\mathrm{K}}\Delta t}{2\eta_{\mathrm{s}}^{\mathrm{K}}} B_s = 1 - \frac{G^{K}\Delta t}{2\eta_{s}^{K}}$.

The new updated mean stress is expressed as:

$$\sigma'^{\mathrm{N}}_{\mathrm{m}} = \frac{1}{a_{\mathrm{m}}}\left[\Delta e_{\mathrm{vol}} + b_{\mathrm{m}}\sigma'^{\mathrm{O}}_{\mathrm{m}} - \left(\frac{B_{\mathrm{m}}}{A_{\mathrm{m}}} - 1\right) e_{\mathrm{vol}}^{\mathrm{K,O}}\right], \tag{18}$$

where $a_{\mathrm{m}} = \frac{1}{K^{\mathrm{M}}} + \frac{\Delta t}{2}\left(\frac{1}{\eta_{\mathrm{m}}^{\mathrm{M}}} + \frac{1}{\eta_{\mathrm{m}}^{\mathrm{K}} A_{\mathrm{m}}}\right)$ $b_{\mathrm{m}} = \frac{1}{K^{\mathrm{M}}} - \frac{\Delta t}{2}\left(\frac{1}{\eta_{\mathrm{m}}^{\mathrm{M}}} + \frac{1}{\eta_{\mathrm{m}}^{\mathrm{K}} A_{\mathrm{m}}}\right)$.

The new updated deviatoric stress is deduced as:

$$S'^{\mathrm{N}}_{ij} = \frac{1}{a_{\mathrm{s}}}\left[\Delta e_{ij} + b_{\mathrm{s}} S'^{\mathrm{O}}_{ij} - \left(\frac{B_{\mathrm{s}}}{A_{\mathrm{s}}} - 1\right) e_{ij}^{\mathrm{K,O}}\right], \tag{19}$$

where $a_{\mathrm{s}} = \frac{1}{2G^{\mathrm{M}}} + \frac{\Delta t}{4}\left(\frac{1}{\eta_{\mathrm{s}}^{\mathrm{M}}} + \frac{1}{\eta_{\mathrm{s}}^{\mathrm{K}} A_{\mathrm{s}}}\right)$, $b_{\mathrm{s}} = \frac{1}{2G^{\mathrm{M}}} - \frac{\Delta t}{4}\left(\frac{1}{\eta_{\mathrm{s}}^{\mathrm{M}}} + \frac{1}{\eta_{\mathrm{s}}^{\mathrm{K}} A_{\mathrm{s}}}\right)$.

Then, the porous creep model is calculated by following the flowchart as shown in Fig. 6.

4.2 TOUGH2-FLAC^{3D} Joint Simulation of the Time-Dependent Hydro-mechanical Coupling Model

A time-dependent hydro-mechanical coupling model was established on the framework of the TOUGH2-FLAC^{3D} coupled simulation by taking advantage of the component-based programming design approach. External modules were designed for joint programs as relatively independent components from TOUGH2 and FLAC^{3D}, which can be compiled, linked, and operated separately. The calculation process can be divided into two phases (Wei et al. 2013): one is the initialization phase necessary to acquire the information pertaining to the initial pore fluid pressure field, temperature field, and initial geostress field; the other involves iterative calculation between Tough2 and Flac^{3D}.

Based on the component-based programming design approach originally proposed by Rutqvist (Rutqvist 2011), disk files were compiled to deliver data in each Newtonian iteration: the data direction and order were controlled by a DOS batch sequence, as well as the entire computational step. The disk data of the whole coupling computation can be divided into the following four categories: pre-processing files, functional files, transitional files, and results files. The pre-processing command files are called to modify the input parameters required for the calculation model and target in Tough2 and Flac^{3D}. Functional files are written to extract the node, element, or stress information from mechanical calculation and a transition file is generated and called by the executable program to exchange data as input or output parameters.

The initialization of the coupling calculation process is conventional for time-dependent and time-independent conditions; however, the mechanical model of iterative calculation in previous research does not consider the time-dependent deformation within the reservoir rock. As a result, the porous creep model is configured in a mechanical simulator. For iterative calculations, Tough2 and Flac^{3D} were used to calculate the results and update the input parameters at each time step. It is worth noting that each time step for the iterative calculation process is different from a creep time step which is an independent iterative process in mechanical property calculation terms.

Moreover, the external module (A) was explored to update the pore pressure and density in input files to mechanical simulation. Meanwhile, the external module (B) was developed to correct these parameters in input files to the Tough2 simulation according to the mechanical calculation results

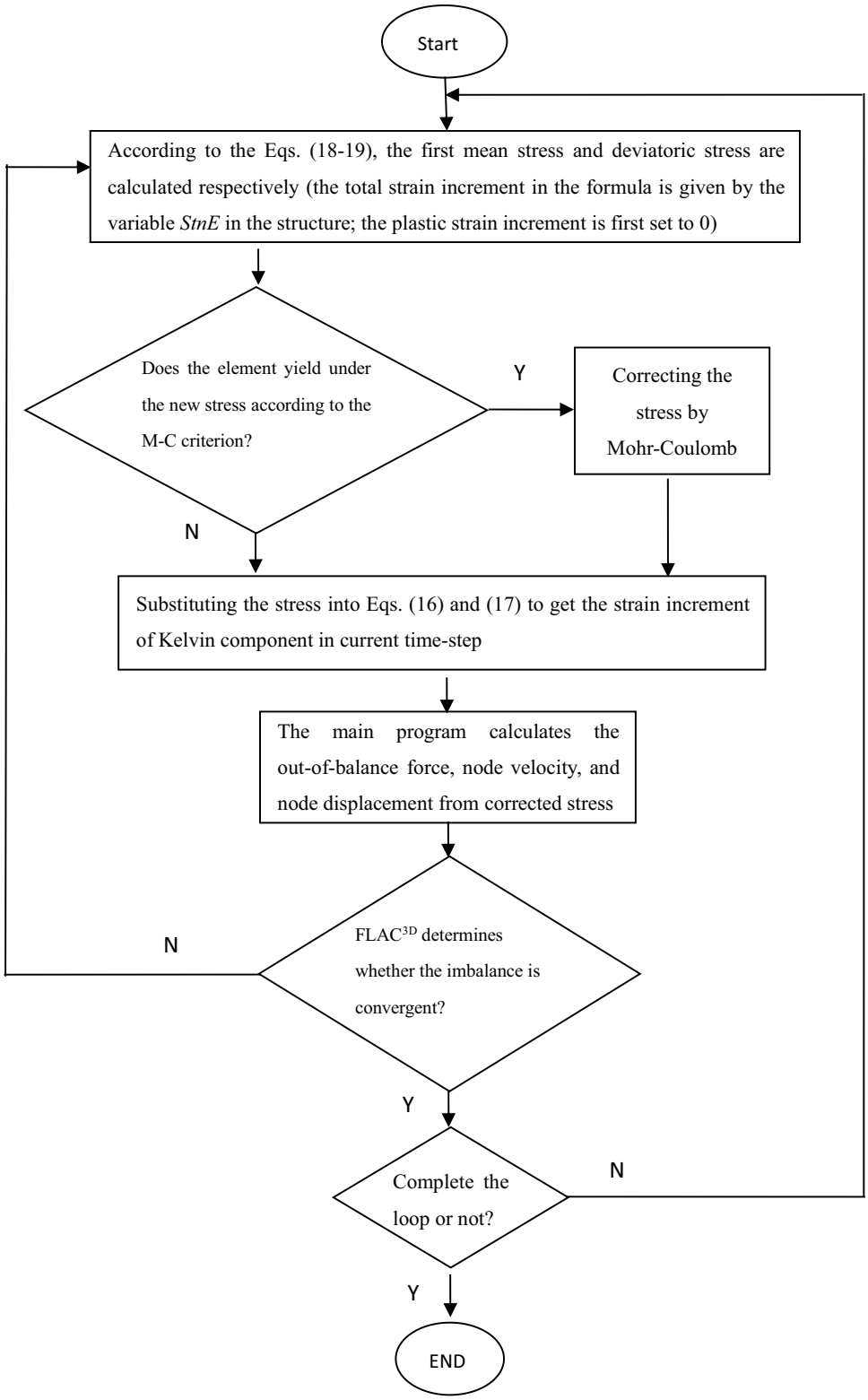

Fig. 6 Flowchart through the porous creep model in FLAC^{3D}

and the evolutionary relationship formula of permeability and porosity. The process of iterative calculation between Tough2 and Flac^{3D} is shown in Fig. 7.

With the application of the iterative calculation between Tough2 and Flac^{3D} equipped with a porous creep model, the long-term deformation and hydraulic properties of reservoir rock during CO_2 injection were evaluated.

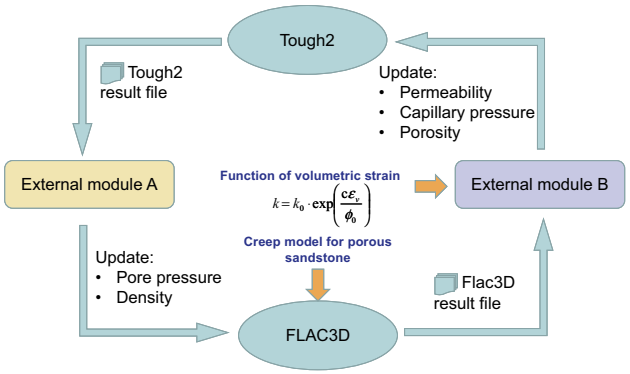

Fig. 7 The process of iterative calculation between Tough2 and Flac^{3D}

According to the initial and boundary conditions in the above experiment, the simulation of a specimen subject to triaxial stress conditions with the flow-through of NaCl solution mixed with CO_2 was demonstrated. The initialization of the geostress field, pore fluid pressure field and geothermal field should be undertaken before the hydro-mechanical coupling process. Based on initialization calculations, the surrounding temperature is about 25 °C, the initial pore pressure P is about 1 MPa and the initial triaxial stresses are the radial pressure σ_2 of 10 MPa and the axial stress σ_1 of 20 MPa. Figure 8 shows the geometric dimensions and simulation conditions.

In the process of NaCl solution with mixed CO_2 penetration, the internal flow-through path in the triaxial test is

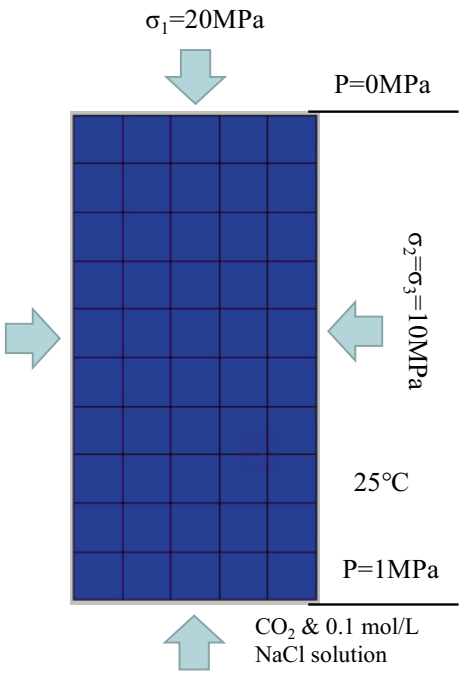

Fig. 8 Dimension and test conditions for the cylindrical specimen

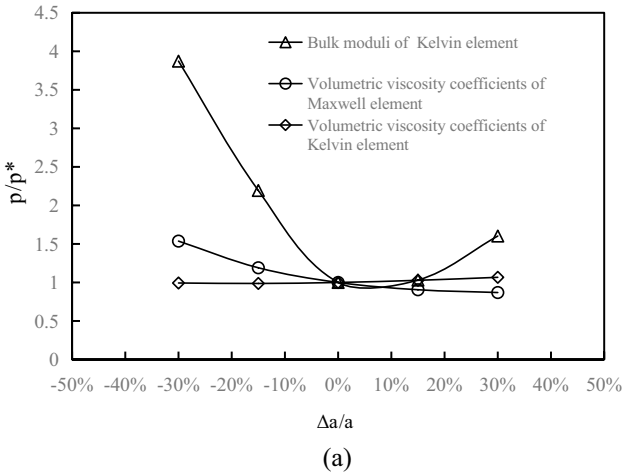

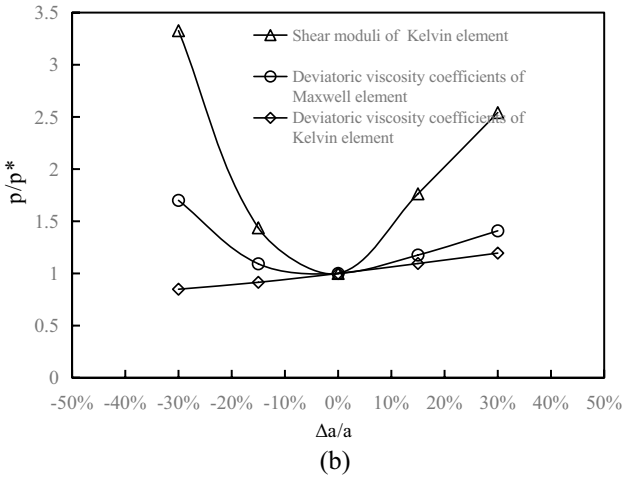

Fig. 9 The sensitivity curves of **a** volumetric parameters and **b** deviatoric parameters

bottom-up. The pressure at the lower end of the rock sample is 1 MPa, and the pressure at the upper end is 0 MPa. Driven by the pore pressure difference, the fluid in the sandstone pores moves upward along the pore channels, and the axial and lateral displacement of the sample can be observed simultaneously: the initial composition of the NaCl solution with mixed CO_2 at the lower end of the rock sample is kept the same as that used in the experiment by specifying the same input parameters such as salinity, temperature, pressure, and potential CO_2 saturation ability.

The model parameters were determined as described in Sect. 3.2. Furthermore, the sensitivity analysis of uncertain parameters was undertaken by setting the objective function of volumetric and deviatoric creep deformation in Eq. (12) as the system characteristic, respectively: the deviations are set to ± 15% and ± 30% in Table 3.

As shown in Fig. 9, under these experimental conditions, the most sensitive parameters affecting the volumetric and deviatoric creep curves are the bulk and shear moduli of

Table 3 Parameters for sensitivity analysis of volumetric parameters and deviatoric parameters

Deviation value	K^K(Pa)	η_m^M(Pa h)	η_m^K(Pa h)	G^K(Pa)	η_s^M(Pa h)	η_s^K(Pa h)
− 30%	6.11×10^{10}	1.98×10^{13}	3.89×10^{11}	1.42×10^{10}	2.97×10^{12}	9.67×10^{10}
− 15%	7.43×10^{10}	2.40×10^{13}	4.72×10^{11}	1.72×10^{10}	3.61×10^{12}	1.17×10^{11}
0	8.74×10^{10}	2.83×10^{13}	5.55×10^{11}	2.03×10^{10}	4.24×10^{12}	1.38×10^{11}
15%	1.00×10^{11}	3.25×10^{13}	6.38×10^{11}	2.33×10^{10}	4.88×10^{12}	1.59×10^{11}
30%	1.14×10^{11}	3.68×10^{13}	7.22×10^{11}	2.63×10^{10}	5.52×10^{12}	1.80×10^{11}

Kelvin elements, respectively; therefore, the parameter calibration is optimized by minimizing the objective function. Combined with other parameters, and referring to previous research (Zheng et al. 2015), in this porous rock, the corresponding model parameters of mechanical calculation are summarized in Table 4. The boundary and initial condition parameters for iterative calculation are summarized in Table 5, and other parameters are set with reference to general settings in Tough2.

Sodium chloride solution at a concentration of 0.1 mol/L is saturated with CO_2 under a constant pressure of 1 MPa at a steady temperature of 25 °C, and the mixed fluid is continually injected at a constant pressure of 1 MPa. As a dilute solution, the density of the mixed fluid is approximately 1 g/cm^3. The solubility of carbon dioxide in10 mmol/L NaCl solution increases with the pressure, so the solubility of carbon dioxide decreases gradually along the flow-through path, and the dissolved carbon dioxide escapes in the form of gas phase at the low-pressure end of the system. The most direct influence of the change in the carbon dioxide phase on the flow-through process is the phase saturation and relative permeability of each phase in the pore. Based on the assumption of isotropic materials and continuous deformation, only one direction of seepage action is considered in the pore fluid migration equation in Tough2. Then, the simulation of the flow-through process is simplified to one dimension.

Table 4 The corresponding model parameters used in mechanical calculation (under a radial pressure of 10 MPa and an axial stress of 20 MPa)

K^M(Pa)	K^K(Pa)	η_m^M(Pa h)	η_m^K(Pa h)	c (MPa)	ϕ(°)
3.25×10^9	9.81×10^{11}	2.83×10^{13}	5.55×10^{11}	7.37	15.42
G^M(Pa)	G^K(Pa)	η_s^M(Pa h)	η_s^K(Pa h)	ψ (°)	σ^t (MPa)
2.49×10^9	2.48×10^{10}	4.24×10^{12}	1.38×10^{11}	0	1.5

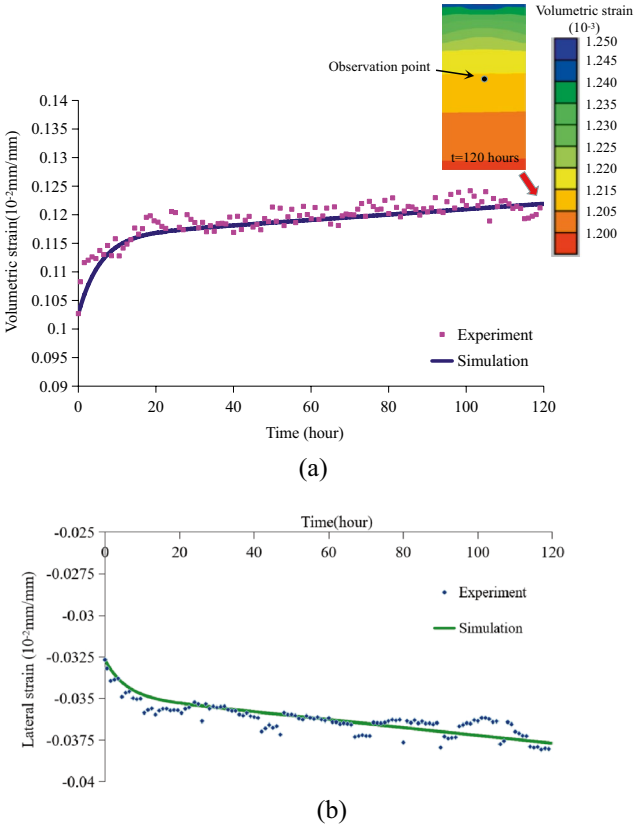

Fig. 10 Comparison of numerical simulation results and experimental results: **a** the volumetric creep curve and **b** the lateral creep curve of sandstone under the flow-through of NaCl solution mixed with CO_2 (under a radial pressure of 10 MPa and an axial stress of 20 MPa)

After 120 h, the iterative calculation had been completed. The volumetric strain was calculated through tracing the deformation data of observation point in the middle cross section of the rock sample and extracting the axial and radial deformation data from the final result file. As shown in Fig. 10, numerical simulation results and experimental

Table 5 The boundary and initial condition parameters for iterative calculation

σ_1 (MPa)	$\sigma_2=\sigma_3$ (MPa)	Pore pressure at the inlet (MPa)	Initial permeability (m^2)	Initial porosity	Initial NaCl concentration (mol/L)	Temperature
20	10	1	4×10^{-18}	0.2135	0.1	25 ℃

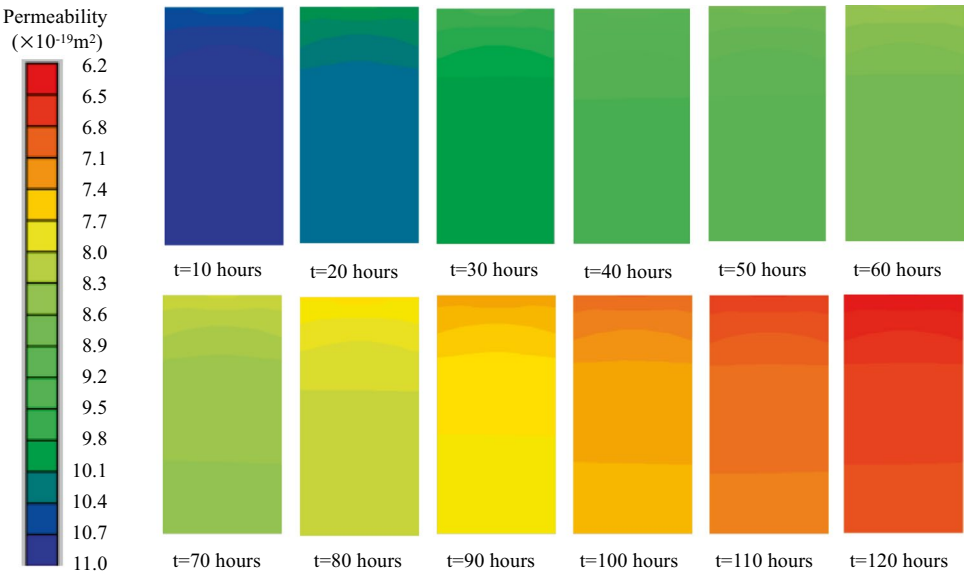

Fig. 11 The evolution of permeability in the vertical section of rock sample at different times

results of volumetric creep curve and lateral creep curve of sandstone under the flow-through of an NaCl solution mixed with CO_2 were compared.

Permeability as an input parameter in Tough2 and the output parameter in the external module B were updated in each iterative loop. During the 120 h of this creep experiment, permeability of the vertical section in the rock sample at different times was extracted from each result. As shown in Fig. 11, the permeability in the representative vertical section zone is decreased with prolonged creep. Results showing the pore pressure gradient is illustrated in Fig. 12: the permeability decreases along the seepage path from the inlet (bottom) to outlet (top) in the corresponding vertical section at each time. This means that the greater the pore pressure to which the zone is subjected, the bigger is the contribution to the volumetric strain from pore expansion and the more permeable is the zone. At the scale of amplification, as shown in Fig. 12b, the evolution of permeability alone the seepage path is demonstrated.

To compare with the hydraulic conductivity of sandstone in experimental results, the outflow data of all the outlet zones in the rock sample in each iterative step were extracted from the result files of Tough2. The hydraulic conductivity was calculated by the flow rate per unit cross-sectional area, differential pore pressure between the bottom and top of the sample, density, and viscosity. As shown in Fig. 13, numerical simulation results and experimental results of hydraulic conductivity of sandstone under the flow-through of an NaCl solution mixed with CO_2 were compared.

To compare data with the simulated results under different stress states, the rock sample from the same source was subjected to a radial pressure σ_2 of 5 MPa, and an axial stress σ_1 of 10 MPa, while the other conditions of the mixed flow-through that are the same as the aforementioned experiment, such as the composition ratio, the surrounding temperature, and the initial pore pressure, were examined. Except for the stress state, the boundary and initial condition parameters are as listed in Table 5. By iterative solution of the data in the previous stage, the model parameters were obtained (Table 6).

As shown in Fig. 14a and b, numerical simulation results and experimental results of volumetric creep curve and lateral creep curve of sandstone under a radial pressure σ_2 of 5 MPa and an axial stress σ_1 of 10 MPa were compared.

By comparing the variations in these parameters of simulation results under different stress states, the increasing consolidation effect of the confining pressure on porous sandstone can be accounted for by the associated increases in the elastic deformation parameters, as well as the decrease in the initial hydraulic conductivity. The parameters with respect to deviatoric viscous behavior and volumetric viscous behavior were affected differently by the stress state. The more compact the material, the harder it was to deform and penetrate.

The volumetric creep curves under different stress states are in good agreement with the experimental data, while the simulated hydraulic conductivity was greater than that measured. The contributions to the changes in porosity and permeability not only come from the mechanical deformation, but also include those arising from mineral dissolution and precipitation. That means the difference may be due to the neglect of any chemical action and its effect on pore structure.

5 Conclusions and Discussion

Porosity and permeability in saline reservoir, as evaluation parameters of the CO_2 storage volume in a saline aquifer and range of CO_2 migration, play a significant role in optimizing

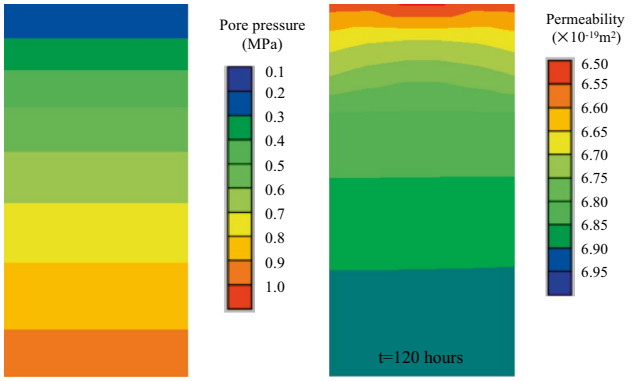

Fig. 12 Pore pressure gradient distribution (**a**) and contour of permeability at 120 h (**b**) in the vertical section of the rock sample

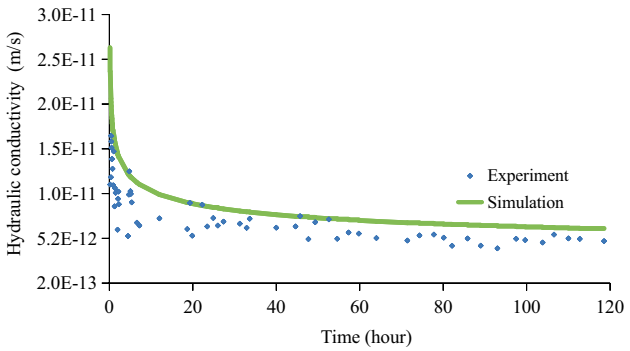

Fig. 13 Comparison of numerical simulation results and experimental results: hydraulic conductivity of sandstone under the through-flow of NaCl solution mixed with CO_2

the injection rate and pressure of CO_2 and assessment of geological carbon storage potential. For long-term processes activated by hydraulics of pore fluid (CO_2 and brine) and mechanics of reservoir rock, the time-dependent influences of evolving permeability and deformation on carbon dioxide geological storage in deep saline aquifer were investigated using different methods.

In test methods, triaxial creep tests with the flow-through of NaCl solution mixed with CO_2 were implemented at a constant 25 °C. As the test results show, both the deformation of reservoir rock and hydraulic conductivity are time dependent: the axial, lateral, and volumetric deformation increased with time, while the hydraulic conductivity diminished with time. Subsequently, based on long-term hydro-mechanical laboratory testing, a theoretical method was utilized by referring to an established time-dependent hydro-mechanical coupling model.

In the theoretical models, the relationship between mechanical process and hydraulic conduction process is generally established as one that includes stress-dependent or strain-dependent permeability. In the view of the mechanics of porous media, porosity is closely related to the deformation of the porous rock skeleton. In this article, based on the porous creep model, permeability was established as the function of volumetric deformation by means of porosity. After CO_2 injection, the formation pressure dissipates and enters normal and constant conditions in the reservoir and the rapid expansion or compression of the storage space does not occur, but, as a material undergoes time-dependent deformation, the reservoir rock is subject to a creep process that also contributes to the changes in its hydraulic conductivity. In consequence, strain-dependent permeability relationships combined with the porous creep model are suitable to describe the long-term evolution of reservoir rock hydro-mechanical coupling processes. Besides the long-term strain-dependent permeability evolution of the reservoir, other problems beyond the scope of this article such as the subsidence caused by groundwater extraction and the creep characteristic of pore geomaterial could be solved by the porous creep model.

The coupled multicomponent multiphase flow and geomechanical simulator TOUGH-FLAC can be applied to verify the time-dependent hydro-mechanical coupling model, including a porous creep model and a time-dependent relationship between permeability and volumetric strain of reservoir rock. Previous studies (Wei et al. 2013; Rutqvist et al. 2006; Rutqvist, 2011) could be referred to for details of the whole iteration and circulation process between TOUGH and FLAC; however, in the present work, only the embedded creep model for porous sandstone in FLAC and the external module to corrected permeability and porosity in input files to the Tough simulation are described as two theoretical innovations. Then, the volumetric deformation was extracted from the result files of $Flac^{3D}$ based on strain data in the lateral and axial directions, and at each iterative step, the outflow data from all the outlet elements in the rock sample were extracted from the result files of Tough2 to calculate the hydraulic conductivity.

As the simulated results under two different stress states, the volumetric creep curves better match the experimental value than the case with the hydraulic conductivity. Along the flow-through path, minerals dissolve in dilute concentration and precipitate in supersaturated condition at solid–liquid contact surfaces; meanwhile, minerals dissolve under higher stress at intergranular contact points and precipitate under lower stress at the free face around the mineral grains. The chemical dissolution and precipitation process occurs between sandstone and the NaCl solution mixed with CO_2; whether it is the pressure dissolution process of particle contact surface or the dissolution and precipitation of pore free surfaces, it will lead to a change in pore volume. Hence, the chemical dissolution and precipitation processes induce little difference to the simulated results and experiment data.

Table 6 The corresponding model parameters used in mechanical calculation (under a radial pressure of 5 MPa and an axial stress of 10 MPa)

K^M (Pa)	K^K (Pa)	η_m^M (Pa h)	η_m^K (Pa h)	c (Pa)	ϕ (°)
3.01×10^9	1.03×10^{11}	2.91×10^{13}	8.72×10^{11}	7.37×10^6	15.42
G^M (Pa)	G^K (Pa)	η_s^M (Pa h)	η_s^K (Pa h)	ψ (°)	σ^t (Pa)
1.64×10^9	1.61×10^{10}	2.48×10^{12}	1.26×10^{11}	0	1.5×10^6

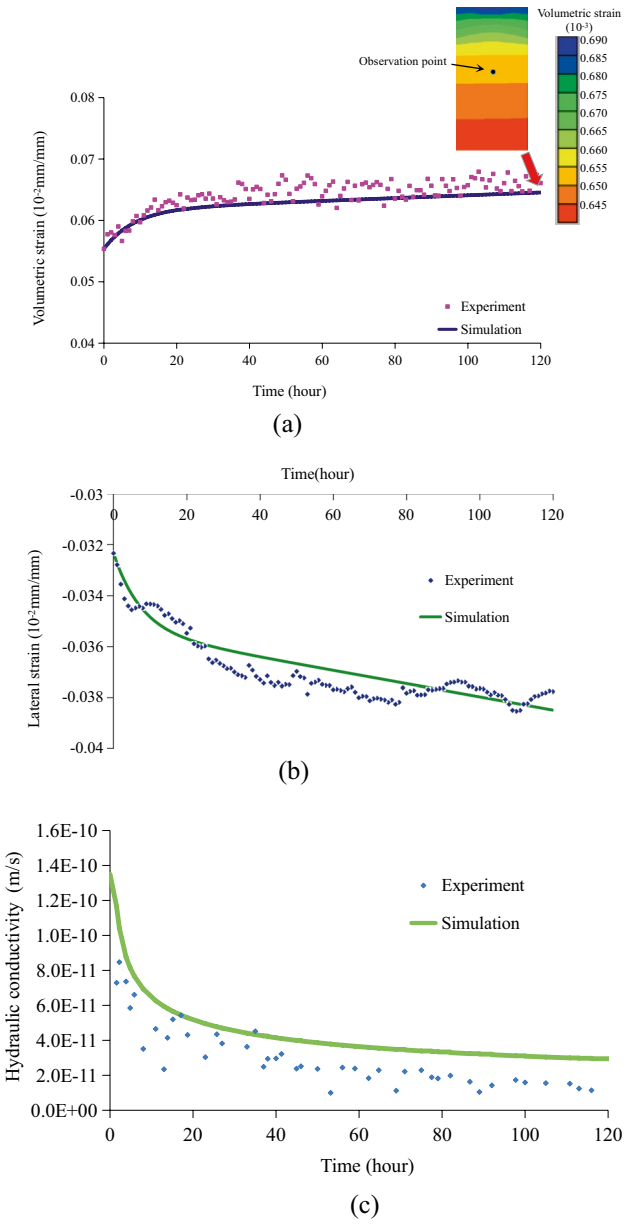

Fig. 14 Comparison of numerical simulation results and experimental results: **a** the volumetric creep curve, **b** lateral creep curve, and **c** hydraulic conductivity of sandstone under the flow-through of NaCl solution mixed with CO_2 (under a radial pressure of 5 MPa and an axial stress of 10 MPa)

Therefore, equipped with the porous creep model and the external module, the capability of the TOUGH-FLAC joint calculation software is demonstrated on time-dependent hydro-mechanical coupled problems related to long-term geological storage of carbon dioxide.

It is noted that the permeability as a function of volumetric strain in Eq. (15) is the absolute permeability, which is an intrinsic property of reservoir rock that does not vary with the properties of the fluid flowing through it. Due to the outflow data acquisition method used during flow-through experiments, hydraulic conductivities derived from the use of Darcy's law were used to describe how easily the liquid phase can pass through the pore skeleton. From a more rigorous perspective, the hydraulic conductivity used herein should be defined as the effective hydraulic conductivity of the liquid phase. Since the gas flow data in the test were not obtained for comparison with data arising from numerical simulation, there is no need to distinguish between the types of hydraulic conductivity used for each of the two phases.

Limited by the lack of field data for geological storage of carbon dioxide within a certain time frame, the feasibility of the time-dependent hydro-mechanical coupled model and its calculation method were verified only on the scale of the available experimental data: however, it provided a new decision-making factor for schematic comparison of the target reservoir from the perspective of long-term permeability evolution. The stronger the time-dependent mechanical properties displayed by the reservoir rock, the smaller is the extent of the spread of carbon dioxide in the reservoir after sealing the well. Therefore, based on the numerical model applied in triaxial creep tests with the flow-through of NaCl solution mixed with CO_2, the time-dependent hydro-mechanical coupling mechanism from experiment and numerical computation method could be applied to the analysis of CO_2 sequestration in deep saline aquifers for long-term evaluation of sequestration potential at large scale. With the application of the iterative calculation process between Tough2 and Flac^{3D}, permeability evolution in the formation rock with changing pore pressure during or after CO_2 injection could be deduced to overcome problems in reservoir storage capacity and caprock impermeability. In consequence, this result provides a theoretical foundation for the demonstration and optimization of site selection, injection scheme, and related parameters in deep CO_2 sequestration operations.

Author contributions HZ conceived the research and all authors contributed ideas thereto. HZ wrote the first draft and all authors helped to revise the manuscript.

Funding We gratefully acknowledge support from the National Natural Science Foundation of China (General Program Grant No. 51879261).

Availability of data and material Not applicable.

Code availability Not applicable.

Declarations

Conflict of interest The authors declare no conflict of interest.

References

Audigane P, Brown S, Dimier A et al (2013) The European FP7 ULTimateCO2 project: A comprehensive approach to study the long term fate of CO2 geological storage sites[C]// Agu Fall Meeting. AGU Fall Meeting Abstracts

Coussy O (2004) Poromechanics. John Wiley & Sons, Chichester

Foroutan M, Ghazanfari E (2020) CO_2-enriched brine injection's impact on mechanical properties of a sandstone specimen. E3S Web Conf 205(2):02005

Foroutan M, Ghazanfari E, Amirlatifi A et al (2020) Variation of pore-network, mechanical and hydrological characteristics of sandstone specimens through CO2-enriched brine injection. Geomech Energy Environ 26(1):100217

Guen YL (2007) Enhanced deformation of limestone and sandstone in the presence of high fluids. J Geophys Res: Solid Earth

Hangx S, van der Linden A, Marcelis F, Bauer A (2013) The effect of CO_2 on the mechanical properties of the Captain Sandstone: Geological storage of CO_2 at the Goldeneye field (UK). Int J Greenhouse Gas Control 19:609–619

Ilgen AG, Newell P, Hueckel T et al (2019) Coupled chemical-mechanical processes associated with the injection of CO_2 into subsurface. Science of carbon storage in deep saline formations. Elsevier, Amsterdam, pp 253–269

Krevor SCM, Pini R, Zuo L et al (2012) Relative permeability and trapping of CO_2 and water in sandstone rocks at reservoir conditions. Water Resour Res. https://doi.org/10.1029/2011WR010859

Lei H, Xu T, Jin G (2015) TOUGH$_2$Biot-a simulator for coupled thermal-hydrodynamic-mechanical processes in subsurface flow systems: application to CO_2 geological storage and geothermal development. Comput Geosci 77:819

Morris JP, Hao Y, Foxall W, McNab W (2011) In Salah CO_2 storage JIP: hydromechanical simulations of surface uplift due to CO_2 injection at In Salah. Energy Procedia 4:32693275

Olden P, Pickup G, Jin M, Mackay E, Hamilton S, Somerville J et al (2012) Use of rock mechanics laboratory data in geomechanical modeling to increase confidence in CO_2 geological storage. Int J Greenh Gas Control 11:304315

Randolph JB, Saar MO (2011) Coupling carbon dioxide sequestration with geothermal energy capture in naturally permeable, porous geologic formations: implications for CO_2 sequestration. Energy Procedia 4:2206–2213

Rutqvist J (2011) Status of the TOUGH-FLAC simulator and recent applications related to coupled fluid and crustal deformation. Comput Geosci 37:739–750

Rutqvist J (2012) The geomechanics of CO_2 storage in deep sedimentary formations. Geotech Geol Eng 30(3):525551

Rutqvist J, Wu YS, Tsang CF et al (2002) A modeling approach for analysis of coupled multiphase fluid flow, heat transfer, and deformation in fractured porous rock. Int J Rock Mech Min Sci 39(4):429–442

Rutqvist J, Birkholzer J, Cappa F (2006) Shear-slip analysis in multiphase fluid-flow reservoir engineering applications using TOUGH-FLAC. In: Proceedings of tough symposium

Rutqvist J, Vasco D, Myer L (2010) Coupled reservoir-geomechanical analysis of CO_2 injection and ground deformations at In Salah, Algeria. Int J Greenh Gas Control 4:225230

Rutqvist J, Liu H-H, Vasco DW, Pan L, Kappler K, Majer E (2011) Coupled non-isothermal, multiphase fluid flow, and geomechanical modeling of ground surface deformations and potential for induced micro-seismicity at the In Salah CO_2 storage operation. Energy Procedia 4:35423549

Rutqvist J, Rinaldi AP, Cappa F, Jeanne P, Mazzoldi A, Urpi L et al (2016) Fault activation and induced seismicity in geological carbon storage lessons learned from recent modeling studies. J Rock Mech Geotech Eng 8(6):789804

Rutqvist J et al (2019) Numerical geomechanics studies of geological carbon storage (GCS), pp 179–189

Seunghee K, Nicolas Espinoza D, Jung J, Cha M, Carlos Santamarina J (2019) Chapter 17—carbon geological storage: coupled processes, engineering and monitoring. In: Newell P, Ilgen AG (eds) Science of carbon storage in deep saline formations. Elsevier, pp 383–407. ISBN 9780128127520, https://doi.org/10.1016/B978-0-12-812752-0.00017-4

Sharifzadeh M, Tarifard A, Moridi MA (2013) Time-dependent behavior of tunnel lining in weak rock mass based on displacement back analysis method. Tunn Undergr Space Technol 38:348–356

Vilarrasa V, Carrera J (2015) Geologic carbon storage is unlikely to trigger large earthquakes and reactivate faults through which CO_2 could leak. Proc Natl Acad Sci USA 112:59385943

Wang W, Kosakowski G, Kolditz O (2009) A parallel finite element scheme for thermo-hydro-mechanical (THM) coupled problems in porous media. Comput Geosci 35(8):1631–1641

Watanabe N, Wang W, McDermott CI et al (2010) Uncertainty analysis of thermo-hydro-mechanical coupled processes in heterogeneous porous media. Comput Mech 45(4):263

Wei Y, Li X, Bing B (2013) The application of the strength reduction method in site stability analysis of CCS. Springer, Berlin Heidelberg

Zheng H, Feng X et al (2015) A creep model for weakly consolidated porous sandstone including volumetric creep. Int J Rock Mech Min Sci. https://doi.org/10.1016/j.ijrmms.2015.04.021

Zoback MD, Gorelick SM (2012) Earthquake triggering and large-scale geologic storage of carbon dioxide. Proc Natl Acad Sci USA 109:1016410168